Nobuaki Kumagai (M'59–SM'71–F'81) was born in Ryojun, Japan, on May 19, 1929. He received the B. Eng. and D. Eng. degrees from Osaka University, Osaka, Japan, in 1953 and 1959, respectively.

From 1956 to 1960, he was a Research Associate in the Department of Communication Engineering at Osaka University. From 1958 through 1960, he was a Visiting Senior Research Fellow at the Electronics Research Laboratory of the University of California, Berkeley, while on leave of absence from Osaka University. From 1960 to 1970, he was an Associate Professor, and has been a Professor of Communication Engineering at Osaka University since 1971. He served as a Department Chairman in the periods of 1972–1973, 1977–1978, and 1983–1984. From 1980 to 1982, he was the Dean of Students of Osaka University.

His fields of interest are electromagnetic theory, microwaves, millimeter waves, and acoustic-waves engineering, optical fibers and optical fiber communication techniques, optical integrated circuits and devices, and lasers and their applications. He has published more than 100 technical papers on these topics in established journals. He is the author or coauthor of several books including *Microwave Circuits* and *Introduction to Relativistic Electromagnetic Field Theory*. From 1979 to 1981, he was Chairman of the Technical Group on the Microwave Theory and Techniques of the Institute of Electronics and Communication Engineers of Japan. He is chairman of the Kinki Regional Broadcast Program Council of the Japan Broadcasting Corporation (NHK), and is the consultant for the Nippon Telegraph and Telephone Public Corporation (NTT).

Dr. Kumagai is a member of the Institute of Electronics and Communication Engineers of Japan, the Institute of Electrical Engineers of Japan, and the Laser Society of Japan. He was awarded an IEEE Fellowship for contributions to the study of wave propagation in electromagnetics, optics, and acoustics.

Design of Waveguide *E*-Plane Filters with All-Metal Inserts

YI-CHI SHIH, MEMBER, IEEE

Abstract—**Waveguide *E*-plane filters with all-metal inserts are designed by a procedure based on the reflection coefficients of axial inductive strips. The scattering matrix, representing the junction in a bifurcated waveguide, is calculated by a mode-matching method. The reflection coefficient for an inductive strip is then obtained by cascading two scattering matrices separated by a distance equal to the stripwidth. The design is valid up to moderate bandwidths, except for the narrowband design at the higher waveguide frequency range, where both the center frequency and the bandwidth are inaccurate. Possible sources of error are studied and a method minimizing the error is proposed.**

I. Introduction

WAVEGUIDE *E*-plane filters with all-metal inserts (Fig. 1) were originally proposed as low-cost mass-producible circuits for microwave frequencies [1], [2]. More recently, they have been designed for millimeter-wave applications through computer-optimization routines based on accurate analyses [3], [4]. The *E*-plane circuit is developed on a metal sheet by photo-etching, pressing, or stamping. The widths of the slot patterns on the metal sheet are equal to the waveguide height; thus, after assembly, the structure consists of several resonators separated by axial inductive strips. Because dielectric losses are absent, the structure has a high transmission Q factor and is suitable for narrow-band high-Q applications.

Manuscript received November 14, 1983; revised February 27, 1984. This work was supported by the Naval Postgraduate School Foundation Research Program.

The author is with the Electrical Engineering Department, Naval Postgraduate School, Monterey, CA 93943.

In computer-aided designs [3], [4], the optimization program finetunes the filter circuit to make the filter performance satisfy a set of specifications. This feature is desirable in millimeter-wave applications because physically finetuning a circuit of small size is a difficult task. With the aid of the optimization program, human effort is minimized in the process of design. The drawback is, however, the expensive computer resources required for each design. Compared with computer optimization, the network synthesis procedures described in [1] and [2] require only minimum computer time to design a filter. In [1], the procedure is based on a low-pass prototype, and therefore gives good results for narrowband design only. In [2], the procedure is based on a distributed prototype and can be used up to a relatively wide bandwidth; it requires, however, several iterations to complete a design. Unlike the optimization program, which is based on an accurate analysis, the synthesis procedure involves some approximations. Although the design examples given in [1] and [2] have been shown to be valid, there is no guarantee that other designs will be valid. It is, therefore, the purpose of this paper to introduce a design procedure with which one can design an *E*-plane filter up to moderate bandwidth and still have confidence in the result.

The design procedure, based on a distributed step-impedance filter prototype, is a modified version of that described by Levy [5] for design of direct-coupled-cavity filters. For a given set of filter specifications, the junction reflection coefficients at the discontinuities are calculated

0018-9480/84/0700-0695$01.00 ©1984 IEEE

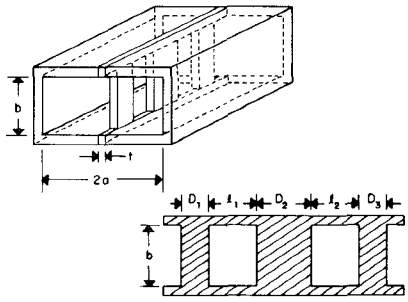

Fig. 1. Geometry of a two-cavity E-plane filter with all-metal inserts.

by explicit formulas; suitable physical junctions that can provide the required reflection coefficients are then chosen and placed at adequate locations to form a filter. The filter performance is approximately predicted by a single formula. In the E-plane filter, the discontinuities are the axial inductive strips. To simplify the process of constructing a filter, we have calculated with a mode-matching method the reflection coefficient of the strip as functions of frequency and stripwidth. The results are collected in several figures in a convenient form for the design.

The range of validity of the design is studied by comparing the predicted filter performances to the performances obtained by an accurate computer simulation. Good agreement is found between them for filters up to moderate bandwidth, except for narrow-band filters designed at the higher waveguide frequency range. Compared with the prediction (by approximation), the simulated result (by accurate analysis) has a lower center frequency, a narrower bandwidth, and a smaller passband ripple. The discrepancy is due to the inaccurate approximation of a wide strip by a lumped reactance and the neglect of the higher order mode coupling between the strips in the design procedure. The problem is serious, but it can be reduced by simply increasing the thickness of the strip or stepping the waveguide sidewalls.

II. Design Procedure

The prototype filter used in this design is the half-wave step-impedance filter as shown in Fig. 2(a). It is a distributed filter consisting of a cascade of n line elements; each element corresponds to a resonator in the conventional filter design. The elements, having characteristic impedances Z_r ($r=1,2,\cdots,n$), are assumed to have an equal length of $l=\lambda_{g0}/2$, where λ_{g0} is the guide wavelength of the line at the center frequency. The electrical response of this transmission-line structure depends upon the impedances of the unit elements. For electromagnetic waves propagating along the line, the impedance differences between the unit elements yield reflected waves which, after appropriate arrangement, will cancel each other at desired frequencies. If, however, a uniform waveguide is used to implement the circuit, all the unit elements are of the same impedance; the necessary wave reflections must be produced by inserting some sort of discontinuities between the unit elements. Fig. 2(b) and (c) shows two such examples where impedance inverters and scattering matrices are inserted as the discontinuities; the unit elements are assumed to have unit impedance. All three circuits will have the same transmission characteristics as long as the following equations hold:

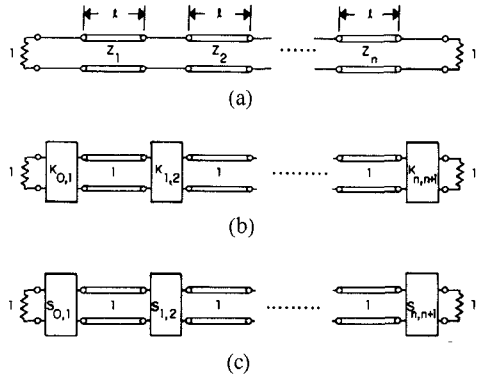

Fig. 2. Filter prototypes. (a) Half-wave step-impedance filter, (b) impedance inverter network, and (c) scattering matrix network.

$$K_{r-1,r}=\sqrt{Z_r/Z_{r-1}} \tag{1}$$

$$(S_{11})_{r-1,r}=\frac{K_{r-1,r}^2-1}{K_{r-1,r}^2+1} \tag{2}$$

where K is the impedance value of the inverter and S_{11} the reflection component in the scattering matrix.

For the prototype filter, an optimum equiripple bandpass response[1] occurs around $\theta=\pi$ when the transmitted power

$$|\bar{S}_{12}|^2=\frac{1}{1+h^2T_n^2\left(\dfrac{\sin\theta}{\alpha}\right)} \tag{3}$$

where

$$\theta=\pi\lambda_{g0}/\lambda_g \tag{4}$$

and

$$T_n(x)=\cosh(n\cosh^{-1}x) \tag{5}$$

is the nth-degree Chebyshev polynomial of the first kind. Alpha (α) defines the passband bandwidth and h defines the passband ripple level.

The network that gives the transfer characteristics in (3) may be obtained by the exact synthesis described in [6]. However, for high-Q narrowband filters, the synthesis procedure suffers from numerical difficulties in reducing the polynomial functions; sophisticated transformation is often required to obtain accurate results. To avoid this problem, we apply the explicit formulas derived by Rhodes [7] for the element values

$$K_{r,r-1}=\sqrt{1+\left(\sin\left[\frac{r\pi}{n}\right]/y\right)^2}\Big/\sqrt{Z_r'Z_{r+1}'}\,, \quad \text{for } r=0,1,\cdots,n \tag{6}$$

with

$$y=\sinh\left[\frac{1}{n}\sinh^{-1}\frac{1}{h}\right] \tag{7}$$

[1]Our discussion is restricted to the equiripple case; a similar discussion can be applied to the maximally flat case.

and

$$Z_r' \begin{cases} = 1, & \text{for } r = 0 \text{ and } n+1 \\ = \dfrac{2\sin\left[\dfrac{(2r-1)\pi}{2n}\right]}{y\alpha} - \dfrac{\alpha}{4y}\left[\dfrac{y^2+\sin^2\left[\dfrac{r\pi}{n}\right]}{\sin\left[\dfrac{(2r+1)\pi}{2n}\right]}\right. \\ \left. + \dfrac{y^2+\sin^2\left[\dfrac{(r-1)\pi}{2n}\right]}{\sin\left[\dfrac{(2r-3)\pi}{2n}\right]}\right], \end{cases}$$

$$\text{for } r = 1, 2, \cdots, n. \quad (8)$$

Equations (6) and (8) omit the higher order power terms in α, and therefore, are only valid up to moderate bandwidths.

In the above discussion, the discontinuities are assumed to be frequency-independent. This assumption is hardly true in practice, especially in waveguide applications. A waveguide discontinuity can usually be represented by a lumped reactive element. For instance, an inductive iris may be represented by a lumped inductor and, for the present case, the axial inductive strip may also be represented by a lumped inductor with appropriate reference planes. The lumped element representation implies that the characteristics of the discontinuity is frequency-dependent and is approximately a linear dependency. The frequency-dependent behavior of the discontinuity has significant effects on the filter performances. In an earlier paper [5], Levy has studied in detail the reactance-coupled filters and concluded that the response in (3) should be modified as

$$|S_{12}|^2 = \frac{1}{1 + h^2 T_n^2\left(\dfrac{\pi \sin\theta}{\theta\alpha}\right)} \quad (9)$$

to take into account the frequency dependence of the discontinuities. Equation (9) accurately predicts the response of reactance-coupled filters up to moderate bandwidths. Based on this expression, a design procedure is as follows.

To design a filter, one is normally given the passband ripple, the stopband attenuation, and the two passband edge frequencies.

The design procedure is as follows:

1) The corresponding guide wavelengths λ_{g1} and λ_{g2} are calculated at the bandedge frequencies. From λ_{g1} and λ_{g2}, the parameters α and λ_{g0} (and therefore, the center frequency f_0) are determined by the following equation:

$$\frac{\lambda_{g1}}{\lambda_{g0}} \sin\frac{\pi\lambda_{g0}}{\lambda_{g1}} = -\frac{\lambda_{g2}}{\lambda_{g0}} \sin\frac{\pi\lambda_{g0}}{\lambda_{g2}} = \alpha. \quad (10)$$

2) If the passband ripple is given as a maximum insertion loss x dB, the parameter h is determined by

$$h = \sqrt{10^{(0.1x)} - 1}. \quad (11)$$

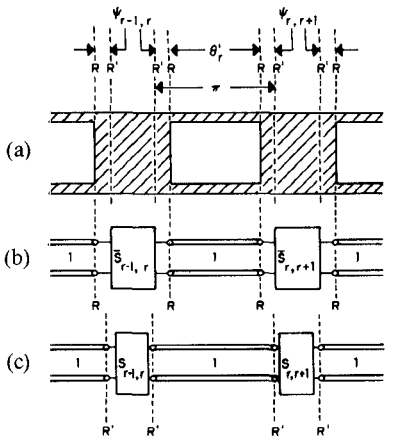

Fig. 3. Relationship between the E-plane structure and its scattering matrix network representations. (a) The E-plane structure, (b) the network representation with reference planes at R, and (c) the corresponding prototype network representation with reference planes at R'.

If it is given as a maximum VSWR, then

$$h = \frac{\text{VSWR} - 1}{2\sqrt{\text{VSWR}}}. \quad (12)$$

3) With the aid of (9), a value of n, the number of unit elements in the filter, will be decided by the stopband attenuation specification.
4) With the parameters α, h, and n, one can obtain the junction reflection coefficient for each discontinuity by the application of (2) and (6)–(8).

We now have the problem of converting these electrical parameters into physical sizes of the E-plane structure. To do this, we consider the scattering matrix network representation of the E-plane structure in Fig. 3. For a lossless junction, the $\bar{S}$ matrix is unitary and reciprocal. Therefore, the $\bar{S}$ matrix is uniquely determined by knowing the magnitude and phase of one of its elements, e.g., the reflection coefficient $\bar{S}_{11}$. In the next section, we will analyze the axial strip of given dimensions to obtain the reflection coefficient; or, inversely, we can determine the dimensions of a strip for a given reflection coefficient. In the numerical calculations, we define the reference planes to be the planes at the edges of the strip. With this particular choice of the reference planes, the resulting reflection coefficient for the axial inductive strip has a phase angle ϕ with a value between $\pi/2$ and π. In the prototype, however, we expect the junction reflection coefficients to be real, i.e., the phase angle is either 0 or π (in this case, π). To compensate for the phase difference, we have to move the reference planes toward the strip for an electrical length

$$\psi = (\pi - \phi)/2. \quad (13)$$

The design procedure is completed therefore by adding the following two steps:

5) For the required reflection level in Step 4, the strip width of each junction is determined from the data provided by a numerical analysis at the center frequency, f_0.
6) The corresponding phase angles for the strips are obtained, from which the resonator lengths (the sep-

arations between the strips) are determined, as shown in Fig. 3, by

$$2\pi l_r/\lambda_{g0} = \theta_r' = (\phi_{r-1,r} + \phi_{r,r+1})/2 \qquad (14)$$

where l_r is the physical length, and θ_r' the electrical length of the rth resonator.

III. Reflection Coefficient of the Inductive Strip

In this section, the problem of an axial inductive strip in a rectangular waveguide is analyzed. The strip is assumed to be located at the center of the guide to reduce the excitation of the even-order modes, and the structure is assumed to be lossless. The reflection coefficients of the inductive strips are calculated and plotted in a convenient form for use with the above design procedure.

Basically, the analysis consists of two parts. Part one deals with a scattering problem in a waveguide bifurcated by a septum of finite thickness (see Fig. 4(a)). A mode-matching method [8] is used to obtain the scattering matrix for the isolated junction. In the second part, two junctions, as in part one, are joined back-to-back to form a finite-width strip, as shown in Fig. 5(a). The overall scattering matrix of the composite structure is obtained by applying a network combination in terms of the generalized scattering matrix. The process takes into account the interaction between junctions by not only the fundamental mode but also all the higher order modes.

A. Bifurcated Waveguide Junction

Consider the bifurcated waveguide in Fig. 4(a), where the septum is located at the center along the E-plane. Because of the symmetry, we can place a magnetic wall at the center along the z-axis and consider only one half of the structure, as shown in Fig. 4(b). The problem becomes a transverse step junction between rectangular waveguides of different widths, a and c. For TE_{no} fields incident from both guides, the total fields in each region are composed of the incident fields and the scattered fields due to the junction. The boundary-value problem is solved by first expanding the total fields in terms of the TE normal modes and then matching the tangential components of the fields at the junction. The amplitudes of the normal modes are conveniently represented by the elements of column vectors as shown in Fig. 4(b), where $(\underline{a}^+, \underline{a}^-)$ and $(\underline{b}^+, \underline{b}^-)$ are the amplitude vectors of the incident and scattered fields in region I and II, respectively. The continuity condition on the tangential components of the electric and magnetic fields is then applied across the aperture ($z = 0$). The resulting equations, with the scattered field amplitudes as unknowns, are rearranged into the form shown in Fig. 4(c). The final solution is the scattering matrix S containing the four elements given by

$$S_{22} = \left[Y_2 + H^T Y_1 H\right]^{-1}\left[Y_2 - H^T Y_1 H\right] \qquad (15a)$$

$$S_{21} = 2\left[Y_2 + H^T Y_1 H\right]^{-1} H^T Y_1 = \left[I - S_{22}\right] H^T \qquad (15b)$$

$$S_{12} = 2\left[H Y_2^{-1} H^T Y_1 + I\right]^{-1} H = H\left[I + S_{22}\right] \qquad (15c)$$

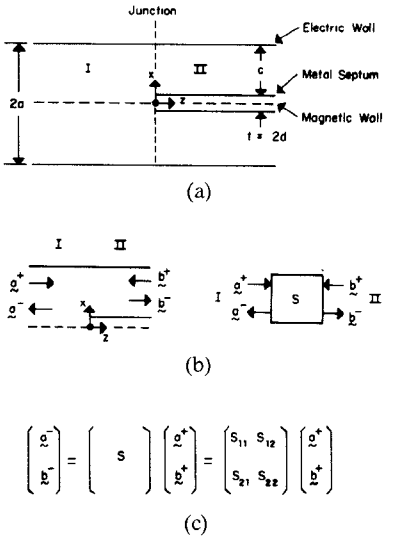

Fig. 4. (a) Junction of waveguide bifurcation, (b) amplitude vector representation for incident and scattered fields, and (c) the generalized scattering parameters.

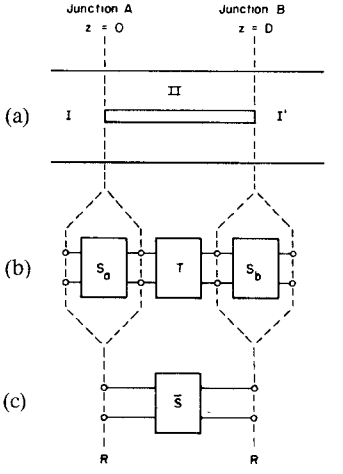

Fig. 5. (a) A septum of width D, (b) scattering network representation, and (c) the composite scattering matrix after network combination.

$$S_{11} = \left[H Y_2^{-1} H^T Y_1 + I\right]^{-1}\left[H Y_2^{-1} H^T Y_1 - I\right] = -H S_{22} H^T \qquad (15d)$$

where I is the identity matrix; Y_1 and Y_2 are diagonal matrices whose diagonal elements are the wave admittances of the corresponding normal modes, defined by

$$Y_1(n,n) = \frac{\gamma_{1n}}{j\omega\mu_0}$$

$$Y_2(n,n) = \frac{\gamma_{2n}}{j\omega\mu_0}, \qquad n = 1,2,\cdots \qquad (16)$$

with

$$\gamma_{1n} = \sqrt{k_n^2 - \omega^2\mu_0\epsilon_0}, \qquad k_n = \frac{(2n-1)\pi}{2a}$$

$$\gamma_{2n} = \sqrt{\left(\frac{n\pi}{2c}\right)^2 - \omega^2\mu_0\epsilon_0} \qquad (17)$$

where $\omega = 2\pi f$ is the angular frequency; μ_0 and ϵ_0 are the

permeability and permittivity of the free space. Matrix H and its transpose H^T are the transformation matrices with the elements defined by

$$H(m,n) = H^T(n,m) = (-1)^n \frac{2}{\sqrt{ac}} \frac{k_m \cos k_m d}{\gamma_{1m}^2 - \gamma_{2n}^2}$$
$$m = 1,2,\cdots, \quad n = 1,2,\cdots. \quad (18)$$

The scattering parameters S_{11}, S_{12}, S_{21}, and S_{22} are matrices containing the scattering characteristics of the fundamental mode, as well as the higher order evanescent modes.

The matrices in (15) are of infinite dimension and the expressions are mathematically exact. However, in practical computations, the matrix size must be truncated, i.e., only a finite number of normal modes can be considered in each region. Let the number of normal modes retained in regions I and II be P and Q, respectively. Then, the dimensions of the matrices Y_1, Y_2, H, H^T, S_{11}, S_{12}, S_{21}, and S_{22} are, respectively, $(P \times P)$, $(Q \times Q)$, $(Q \times P)$, $(P \times P)$, $(P \times Q)$, $(Q \times P)$, and $(Q \times Q)$. The ratio between P and Q is maintained as close as possible to be

$$\frac{P}{Q} = \frac{a}{c} \quad (19)$$

to avoid the relative convergence problem [8]. The value of P is increased until a satisfactory result is obtained. For the cases of our interest, a value of $P = 30$ has been found to yield results better than 0.1 percent.

B. Finite-Width Strip

With the knowledge of the scattering parameters for a single junction, the overall composite scattering matrix can be obtained by a network combination in terms of the generalized scattering matrices, as shown in Fig. 5. Let S_a and S_b represent the scattering matrices for the isolated junctions A and B, respectively. From (15), we obtain the element values for both matrices. Since the characteristics of these two junctions are essentially the same except for the opposite orientation, we have

$$S_{a11} = S_{b22} = S_{11}$$
$$S_{a12} = S_{b21} = S_{12}$$
$$S_{a21} = S_{b12} = S_{21}$$
$$S_{a22} = S_{b11} = S_{22}. \quad (20)$$

Notice that, for the two-port networks, port 1 is defined to be the port on the left-hand side and port 2 on the right-hand side. We now define the T matrix

$$T = \begin{bmatrix} I & 0 \\ 0 & T_2 \end{bmatrix} \quad (21)$$

where I and 0 are the identity matrix and the zero matrix, respectively, and the element matrix T_2 represents the wave propagating (for propagating modes) or attenuating (for evanescent modes) for a distance of D in guide region II. T_2 is a diagonal matrix whose diagonal elements are

$$T_2(n,n) = e^{-\gamma_{2n}D}, \quad n = 1,2,\cdots. \quad (21a)$$

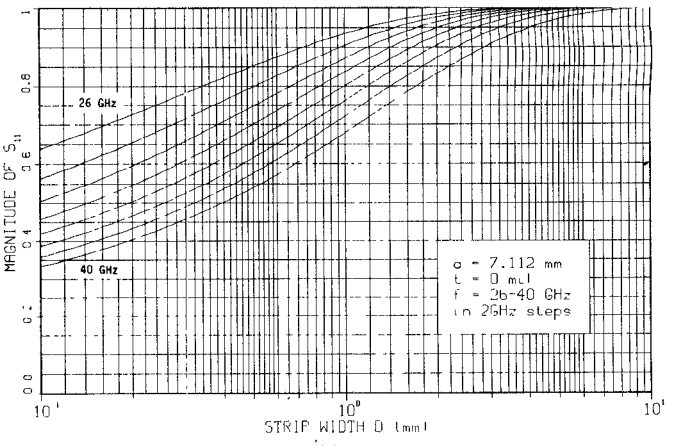

(a)

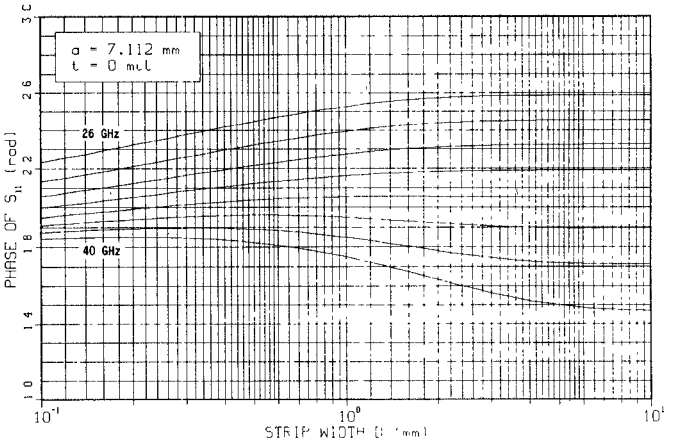

(b)

Fig. 6. Magnitude and phase of the reflection coefficient for inductive strips of thickness $t = 0$.

The combination of matrices S_a, T, and S_b results in the composite scattering matrix $\bar{S}$ for the strip of length D, with the reference planes located at $z = 0$ and $z = D$. As a result, the expression for the reflection coefficient is

$$\bar{S}_{11} = S_{11} + S_{12}T_2S_{22}[I - T_2S_{22}T_2S_{22}]^{-1}T_2S_{21}. \quad (22)$$

Of course, $\bar{S}_{11}$ is still a matrix. We are only interested in the first element $\bar{S}_{11}(1,1)$, which is the fundamental reflection coefficient due to a fundamental incident field.

C. Reflection Coefficients

Based on the above analysis, we can calculate the reflection coefficient of an axial strip for any given dimensions. In the design, however, we need to determine the dimensions of the inductive strips for given reflection coefficients. For this purpose, we have tabulated many sets of data relating the strip dimensions to the reflection coefficient. Due to the space limitation, we only present the data for direct application to the Ka-band design. For other frequency ranges, however, the data can still be applied after appropriate scaling in dimensions.

In the calculations, the strip thicknesses are chosen to be $t = 0$, 1, 2, 5, and 50 mils, and the results are plotted in Figs. 6–10. Both the magnitude and phase of the reflection coefficient are presented as functions of strip width D for

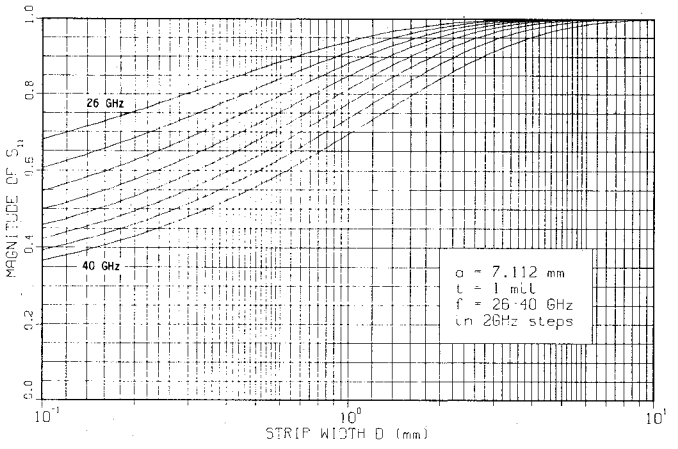

(a)

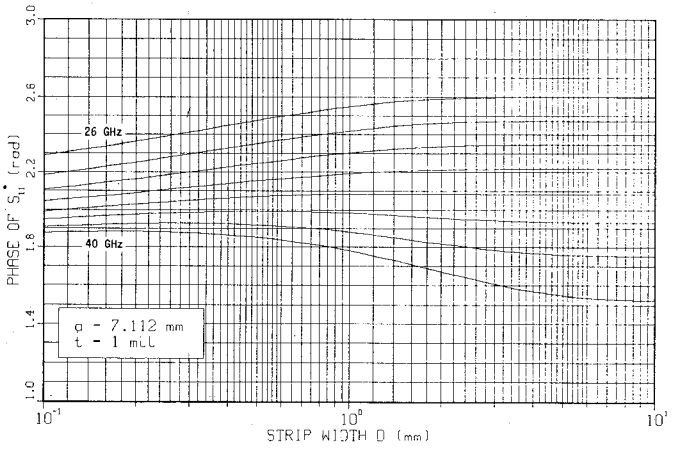

(b)

Fig. 7. Magnitude and phase of the reflection coefficient for inductive strips of thickness $t = 1$ mil.

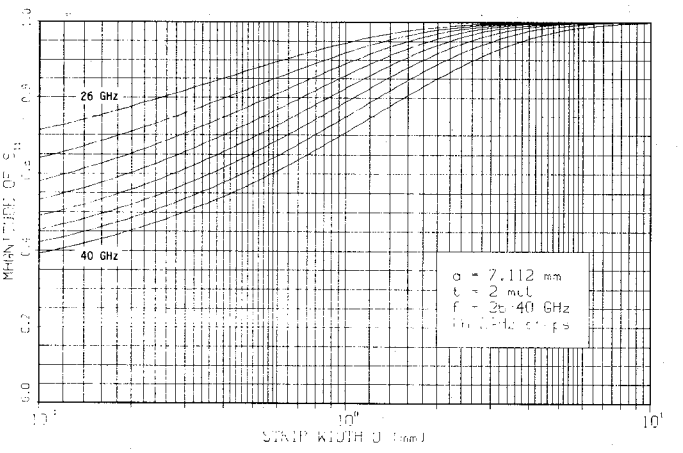

(a)

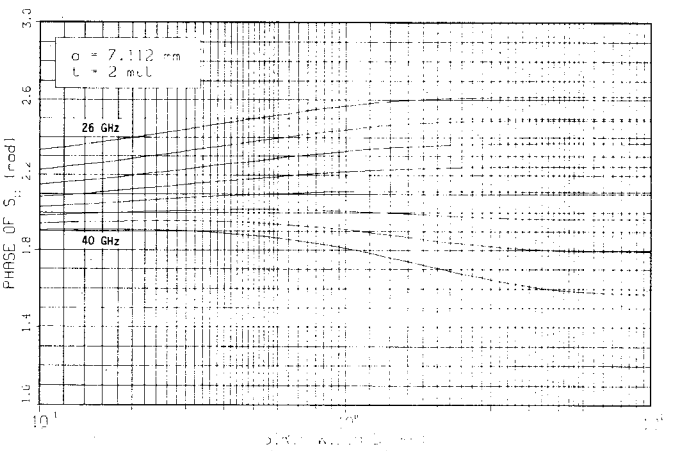

(b)

Fig. 8. Magnitude and phase of the reflection coefficient for inductive strips of thickness $t = 2$ mils.

frequencies running from 26 to 40 GHz in 2-GHz steps. A logarithmic scale is used for D to increase the reading's accuracy for small values of D.

IV. Discussion

The range of validity for the E-plane filter design is limited by two factors. One factor is the dimensional tolerance that is required for reliable and reproducible design. The other factor is the applicable range of the design procedure because of the approximations made in the derivation.

In the present prototype circuit, the reflection coefficients of the discontinuities are symmetrically distributed, with the outermost junctions having the smallest reflection coefficient. The resulting filter design is therefore a symmetrical structure with the outermost strips the narrowest strip. With other design parameters fixed, these strips become narrower as the design bandwidth increases. A maximum available bandwidth is reached when the narrowest strip reaches a tolerable minimum value. If we choose the minimum value to be 0.1 mm (≈ 4 mils), the maximum available bandwidth is calculated and plotted in Fig. 11 as a function of frequency for four passband ripple levels. The number of cavities in the filter n is varied as a parameter. In the calculations, the bandwidth is defined by

$$BW = (f_2 - f_1)/f_0 \tag{23}$$

where f_1 and f_2 are the bandedge frequencies, and f_0 is the center frequency. From the figures, it is noticed that the maximum bandwidth increases with the frequency and, at any frequency, a wider bandwidth can be obtained by increasing the passband ripple level or the cavity number n. The bandwidth increases steadily with the increasing passband ripple level. The increase of n beyond $n = 5$, however, has no significant improvement in bandwidth. The results in Fig. 11 are calculated with a zero-thickness strip. For a thick strip, the maximum available bandwidth is reduced.

The design procedure is approximate because of the omission of the higher order α terms in (6), the approximation of the axial strip by a lumped inductor, and the neglect of the higher order mode coupling between the strips. By comparing to the exact synthesis [6], (6) has been found to yield reflection coefficient values, within the limited maximum bandwidth described above, accurate enough to have no effect on the filter performance. The validity of the design procedure and the filter performance predicted by (9) is mainly dependent on the other two

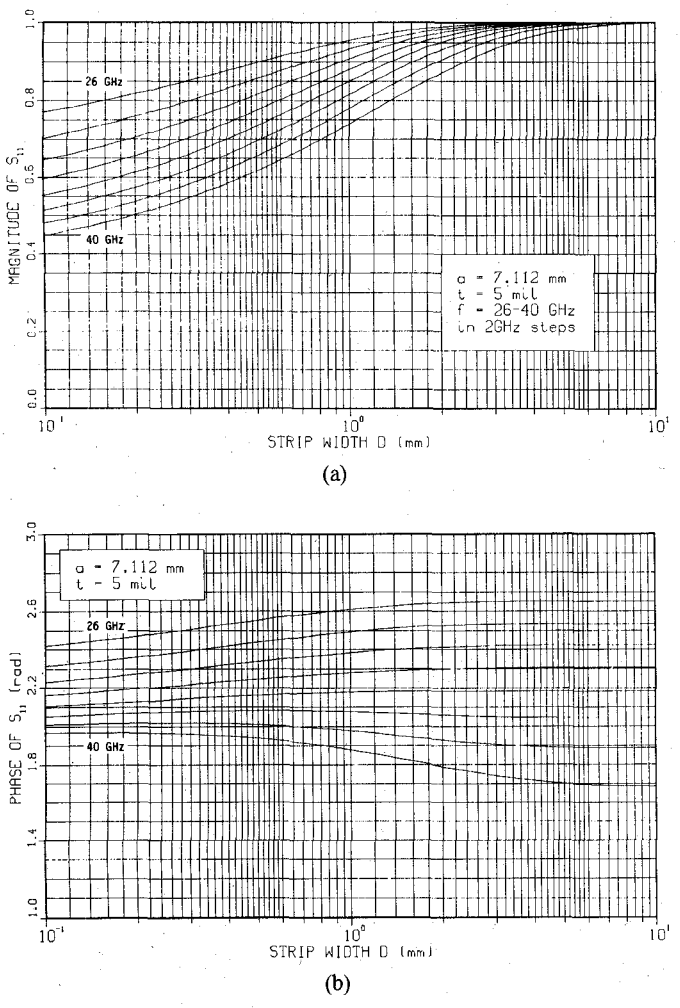

Fig. 9. Magnitude and phase of the reflection coefficient for inductive strips of thickness $t = 5$ mils.

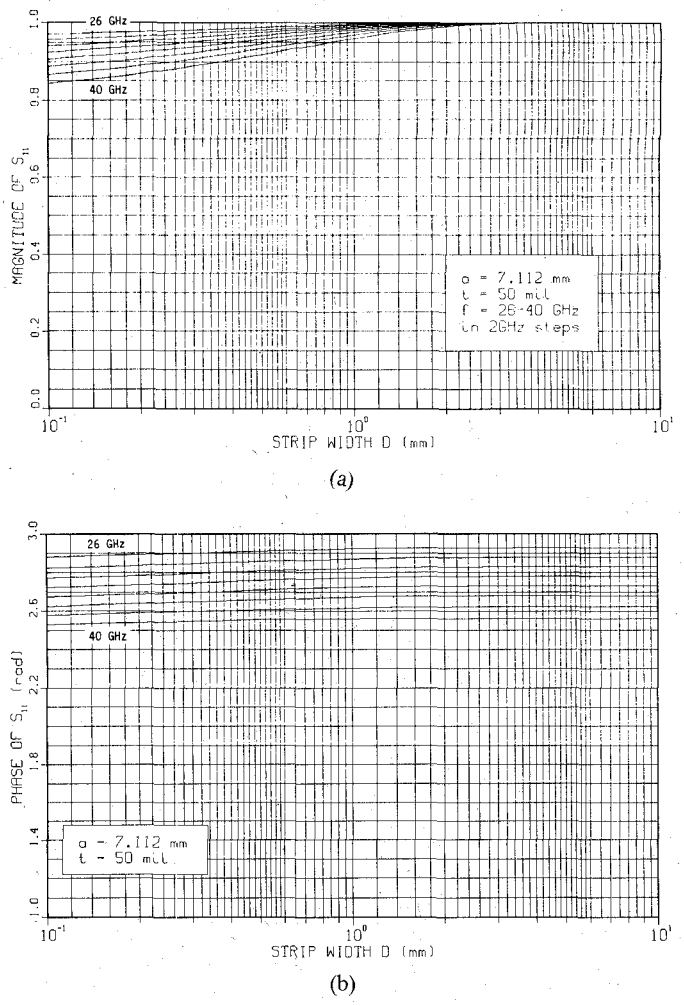

Fig. 10. Magnitude and phase of the reflection coefficient for inductive strips of thickness $t = 50$ mils.

factors. It is impractical for us to verify the design procedure by experimentally making and testing a large number of filters; therefore, an analytical tool is developed by extending the analysis to consider a filter structure consisting of any number of inductive strips. The process, carried out by cascading the scattering matrices that represent the strips, is described in [9]. For a filter of given dimensions, the complete analysis accurately simulates its transmission characteristics, taking into account the correct behavior of each strip and the higher order mode coupling between the strips.

To test the validity of the procedure, hundreds of filters have been designed in Ka band for $n = 2$ to 7 elements having passband ripple levels from 0.05 to 0.5 dB and bandwidths ranging from 0.5 percent up to the maximum available bandwidth. The computed response of each filter by the analysis is then compared with the predicted response given by (9). It is found that the bandedge frequencies, the passband ripple level, and the stopband attenuation are in good agreement, except in the cases when the design bandwidth is close to the maximum available bandwidth and when the center frequency is above about 32 GHz. Two typical designs of relatively wide bandwidths are shown in Fig. 12, where the solid curve is the result by (9) and the dashed curve by the analysis. It is noticed that the bandedge frequencies and the stopband attenuation are in good agreement, except that the errors in the approximated design tend to produce a slightly higher ripple level in practice.

From consideration of the many designs, there exists a tendency that the discrepancy between the filter performance obtained by (9) and by the analysis increases as the design frequency increases. The discrepancy becomes significant in narrowband designs above about 32 GHz. For example, Fig. 13(a) shows a typical design centered at 38 GHz with 0.1-dB ripple level and 1-percent bandwidth. The actual filter response (i.e., the dashed curve computed by the analysis), however, has a 0.7-percent bandwidth and is centered at 37.88 GHz. The error occurs because of the inaccurate approximation of the wide strip by a lumped inductor and the higher order model coupling between the strips.

We have assumed that, in the prototype circuit, no higher order mode could exist; in practice, however, an infinite number of higher order modes exist, in addition to the fundamental mode. Although they do not propagate (i.e., they are evanescent), significant electrical coupling could occur when two strips are "electrically" close. When

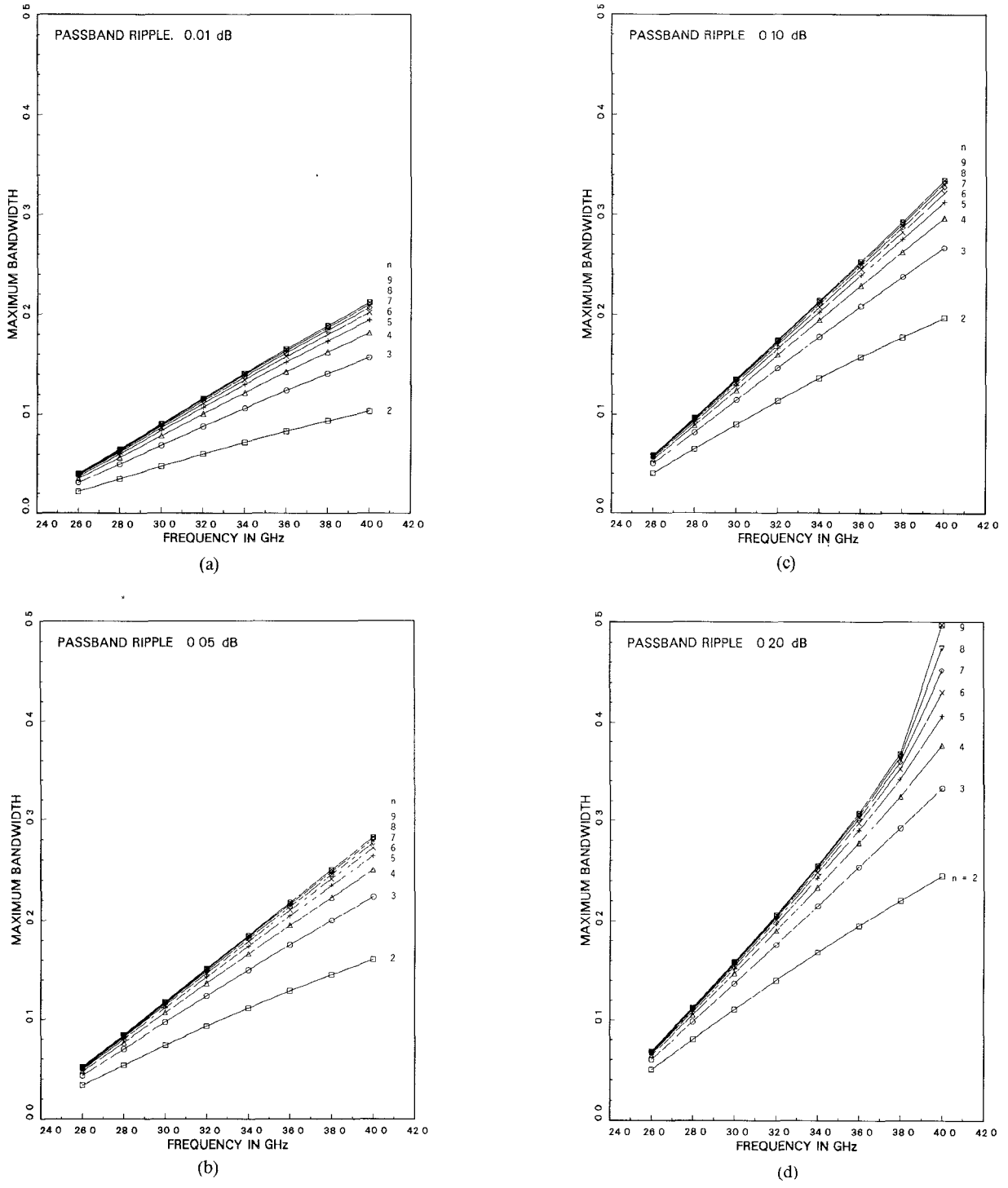

Fig. 11. Maximum available bandwidth of E-plane filters with all-metal inserts

the operating frequency is low, the higher order modes attenuate very rapidly and, therefore, the separation between the strips, approximately equal to one-half of the guide wavelength, is considered electrically very far. As the frequency increases, the electrical distance between the strips is effectively shortened by two main factors. First, the higher order modes attenuate slower and extend their influence to a farther distance. Second, as can be observed from Figs. 6–10, the phase angle of the reflection coefficient decreases when the frequency increases. As a result, the physical and electrical separations between the strips in the filter are shortened according to (14). With these combinations, the filter performance is significantly altered by the higher order mode coupling as the design frequency increases.

The effect due to the higher order mode coupling alone can be demonstrated by using an analysis considering only the fundamental mode in the resonator region. For the same parameters in the previous example, the result is shown in Fig. 13(b) in comparison with the prototype

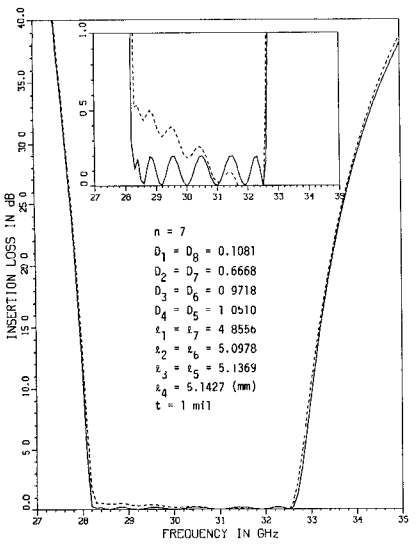

(a)

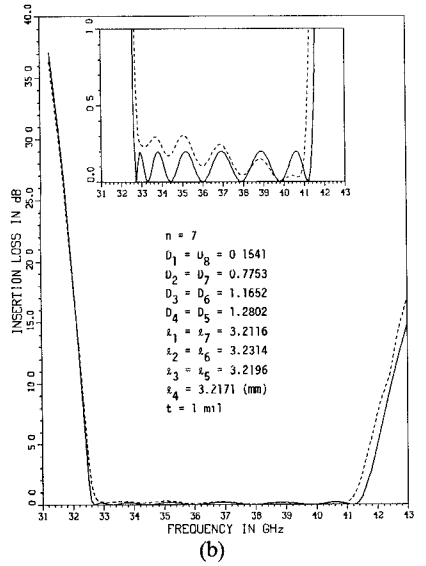

(b)

Fig. 12. Design examples of filters with relatively wide bandwidth.

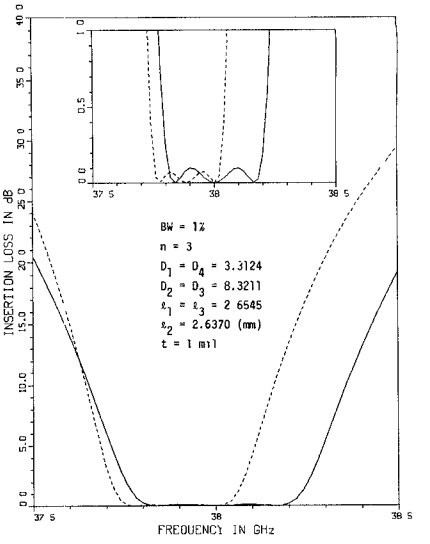

(a)

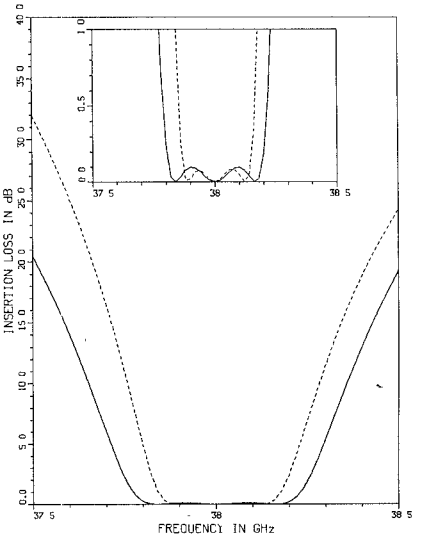

(b)

Fig. 13. Design example of a narrow-band filter at 38 GHz. The predicted filter performance by (9) is compared with that by a complete analysis (a), and with that by an analysis without considering the higher order mode coupling (b).

response by (9). By comparing Fig. 13(a) with Fig. 13(b), it is concluded that the higher order mode coupling is mainly responsible for the shift in the center frequency. The stopband attenuation at higher frequencies is also slightly reduced, but essentially no effect on the bandwidth and passband ripple level is observed. The error in bandwidth is caused by the inaccurate approximation of the frequency behavior for a wide axial strip by a lumped inductor. The approximation gets worse as the strip becomes wider. Unfortunately, the construction of the *E*-plane filters always requires relatively wide strips to produce large junction reflection coefficients. For narrow-band design, especially at higher frequencies, the strip could become so wide that (9) no longer predicts accurate bandwidths. It predicts bandwidths that are too wide. The example in Fig. 13 is one such case—it contains two inductive strips as wide as 8.32 mm. For filters of wider bandwidth, this problem is less serious because of the reduced strip width in the design. For instance, if we refer to Fig. 12(b) for the 24-percent bandwidth filter, the bandwidth is only reduced by 1.6 percent in practice; the widest strip in the design is 1.28 mm.

Equation (9) will predict the bandwidth more accurately if a correction factor is introduced similar to the one derived in Appendix I of [10] and further discussed in [11]. This factor enables a correction between the frequency dependence of a lumped inductive element as compared to the quasi-distributed inductive element. In the present case, however, the correction factor is a complicated function of dimensions and frequency, and is not analytically tractable. Besides, the error in predicting the center frequency still remains because of the higher order mode coupling. Therefore, instead of providing the correction factor, we discuss in the following two possible ways of alleviating the problem.

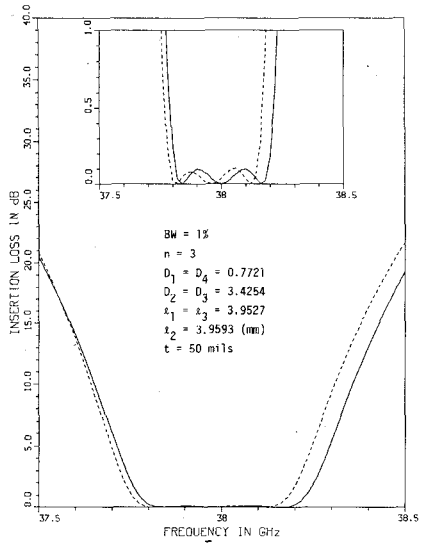

Fig. 14. Design example of a narrow-band filter at 38 GHz with a 50-mil-thick metal insert.

The error involved in the center frequency and the bandwidth of the design at higher frequencies is a serious problem for narrow-band *E*-plane filters. The key to the solution is to minimize the stripwidths and maximize the separations between the strips in a design. Studying the results in Figs. 6–10, we have concluded that a simple solution is to design with a thicker strip. For example, suppose we are to choose a strip to produce a reflection coefficient of magnitude 0.95 at 38 GHz. Using a 1-mil-thick metal, the required stripwidth is 3.1 mm and the associated phase angle of the reflection coefficient is 1.78; while using a 50-mil-thick metal, the stripwidth is 0.68 mm and the phase angle is 2.61. Therefore, if we redesign the 1-percent bandwidth filter at 38 GHz using 50-mil-thick strips, the resulting structure has narrower strips and wider separations as given in Fig. 14. Notice that the result given by (9) (the solid curve) is now in good agreement with that computed by the analysis.

Another possible method for alleviating the wide strips and close spacings is to reduce the waveguide width in the vicinity of the inductive strips in question. The reduced-width waveguide has a higher cutoff frequency and a longer guide wavelength at the same operating frequency. Furthermore, for the same reflection coefficient, the required stripwidth becomes narrower as compared to the original structure. As a result, narrow strips and adequate spacings can be used in a design. The problem is, however, that the effect of the step-wall discontinuity has to be considered in order to obtain accurate results. This problem is being studied.

V. Conclusion

This paper presents a simple design procedure for *E*-plane filters with all-metal inserts. With the aid of the given information on the reflection coefficient of the inductive strip, one can design a filter using a hand calculator. The equation in (9) predicts quite well the filter performances up to a moderate bandwidth, except for the cases of narrow-band filters designed at the higher waveguide frequency range. In those filters, wide metal strips are placed relatively close to each other. Therefore, the higher order mode coupling between the strips and the inaccurate approximation of the wide strips by lumped inductors result in a considerable downward shift in the center frequency and a reduction in the passband bandwidth. Although no better model has been proposed that can fully take into account these problems, we suggest the use of a thicker metal strip for narrow-band design at higher frequencies to reduce these effects.

References

[1] Y. Konoshi and K. Uenakada, "The design of a bandpass filter with inductive strip-planar circuit mounted in waveguide," *IEEE Trans. Microwave Theory Tech.*, vol. MTT-22, pp. 869–873, Oct. 1974.

[2] Y. Tajima and Y. Sawayama, "Design and analysis of a waveguide-sandwich microwave filter," *IEEE Trans. Microwave Theory Tech.*, vol. MTT-22, pp. 839–841, Sept. 1974.

[3] Y. C. Shih and T. Itoh, "*E*-plane filters with finite-thickness septa," *IEEE Trans. Microwave Theory Tech.*, vol. MTT-31, pp. 1009–1013, Dec. 1983.

[4] R. Vahldieck, J. Bornemann, F. Arndt, and D. Grauerholz, "Optimized waveguide *E*-plane metal insert filters for millimeter-wave applications," *IEEE Trans. Microwave Theory Tech.*, vol. MTT-31, pp. 65–69, Jan. 1983.

[5] R. Levy, "Theory of direct-coupled-cavity filters," *IEEE Trans. Microwave Theory Tech.*, vol. MTT-15, pp. 340–348, June 1967.

[6] R. Levy, "Tables of element values for the distributed low-pass prototype filter," *IEEE Trans. Microwave Theory Tech.*, vol. MTT-13, pp. 514–536, Sept. 1965.

[7] J. D. Rhodes, "Design formulas for stepped impedance distributed and digital wave maximally flat and Chebyshev low-pass prototype filters," *IEEE Trans. Circuits Syst.*, vol. CAS-22, pp. 866–874, Nov. 1975.

[8] Y. C. Shih and K. G. Gray, "Convergence of numerical solutions of step-type waveguide discontinuity problems by modal analysis," in *1983 IEEE/MTT-S Intl. Microwave Symp. Dig.*, May 1983, pp. 233–235.

[9] Y. C. Shih, T. Itoh, and L. Q. Bui, "Computer-aided design of millimeter-wave *E*-plane filters," *IEEE Trans. Microwave Theory Tech.*, vol. MTT-31, pp. 135–142, Feb. 1983.

[10] G. F. Craven and C. K. Mok, "The design of evanescent mode waveguide bandpass filters for a prescribed insertion loss characteristic," *IEEE Trans. Microwave Theory Tech.*, vol. MTT-19, pp. 295–308, Mar. 1971.

[11] R. V. Snyder, "New application of evanescent mode waveguide to filter design," *IEEE Trans. Microwave Theory Tech.*, vol. MTT-25, pp. 1013–1021, Dec. 1977.

Yi-Chi Shih (S'79–M'82) was born in Taiwan, the Republic of China, on February 8, 1955. He received the B.Sc. degree from National Taiwan University, Taiwan, R.O.C., in 1976, the M.Sc. degree from the University of Ottawa, Ontario, Canada, in 1980, and the Ph.D. degree from the University of Texas at Austin, in 1982, all in electrical engineering.

In September 1982, he joined the faculty at the Naval Postgraduate School, Monterey, CA, as an Adjunct Professor of Electrical Engineering.